Energy & Environmental Science

Accepted Manuscript

ROYAL SOCIETY OF CHEMISTRY

www.rsc.org/ees

TOC:

The theoretical model for grating structured triboelectric nanogenerators is provided, which outlines its structural and material optimization strategies.

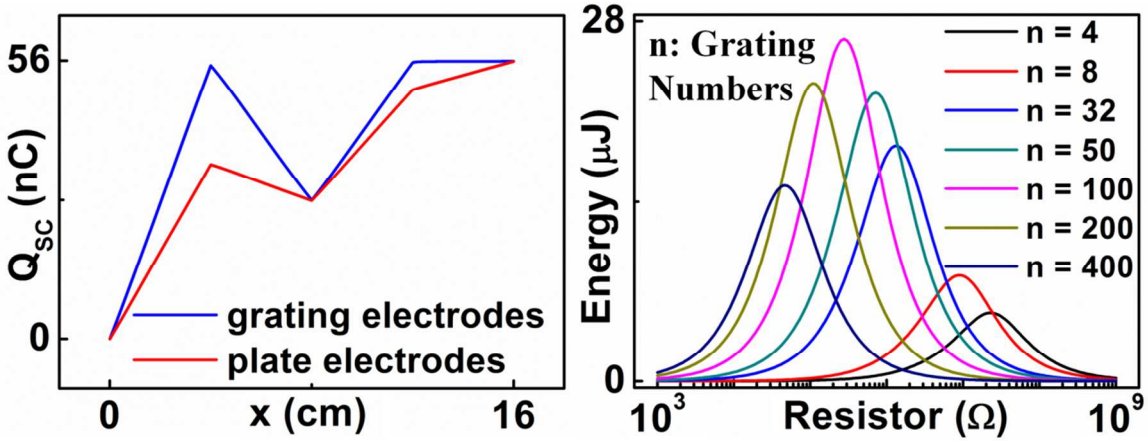

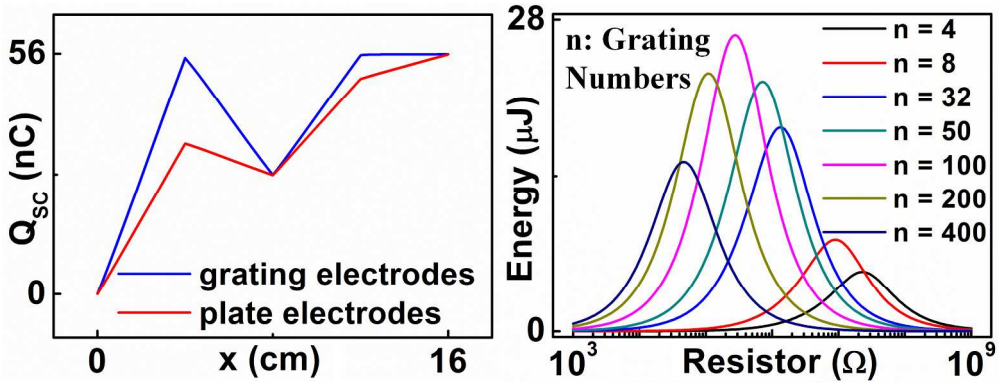

791x300mm (96 x 96 DPI)

Cite this: DOI: 10.1039/c0xx00000x

www.rsc.org/xxxxxx

ARTICLE TYPE

Theoretical Study of Grating Structured Triboelectric Nanogenerators

Simiao Niu, [‡,a] Sihong Wang, [‡,a] Ying Liu, [‡,a] Yu Sheng Zhou,[a] Long Lin,[a] Youfan Hu,[a] Ken C. Pradel,[a] and Zhong Lin Wang[a,b,*]

Received (in XXX, XXX) Xth XXXXXXXXX 20XX, Accepted Xth XXXXXXXXX 20XX

DOI: 10.1039/b000000x

Triboelectric nanogenerator (TENG) technology is an emerging new mechanical energy harvesting technology with numerous advantages. Amongst of the multitude of TENG designs, the grating structure is the most promising for ultra-high output power but also the most complicated. In this manuscript, the first theoretical model of the grating TENG is presented with in-depth interpretation and analysis of its working principle. Two different categories of grating TENGs -- grating TENGs with equal plate-length and with unequal plate-length are discussed in detail to illustrate their difference in output characteristics. Then for each of these two categories, a study of the basic output profiles and an in-depth discussion on the influence of electrode structure, number of grating units, and thickness of the dielectric layers were made to obtain a strategy for optimization.

1. Introduction

Energy harvesting from ambient environment has long been considered as an attractive supplement to traditional power sources. On a large scale, it can assist in solving the current fossil fuel crisis; on a small scale, it can serve as an energy source for sensor networks and portable electronics. Mechanical energy is a universally available source of ambient energy, but is typically neglected and wasted. Traditional mechanical energy harvesting technology harnessed electromagnetic,[1, 2] electrostatic,[3-5] and piezoelectric effects,[6] each of which has its own limitations. Electromagnetic generators rely on necessary heavy permanent magnets and electrostatic electret generators require a pre-charging process. The first nanogenerators were piezoelectric, but the conversion efficiency of these materials remains low. Recently, triboelectric nanogenerators (TENGs) based on contact electrification[7-10] and electrostatic induction overcome the above limitations and exhibit unique merits including large output power, high efficiency, light and cost effective materials, and simple fabrication.[11] As a result, TENGs with various structures have been designed for a wide variety of energy harvesting applications.[11-15] Among them, the grating structure[14, 15] based on in plane charge separation is one of the most effective configurations because of the efficient charge transfer from the multiple in-plane charge separation cycles. However, there are still many mysteries about the grating structure TENG, which hinders the optimization of its performance. First, the detailed output characteristics of this structure are not clear yet. Second, intuitively, a finer structure could enhance its performance, but the validity of this statement still needs to be systematically studied. Finally, the route for optimizing the structural parameters and materials is still unclear. To address these issues, a comprehensive theoretical study of this structure is essential.

In this paper, in-depth theoretical models of two types of grating TENGs, one with equal length plates and the other with unequal length plates, are discussed in detail. Through theoretical and computational methods, their output characteristics are obtained and analysed. With this basic understanding of the output performance, the effect of finer pitches is outlined for both grating structures. In addition, structural and material optimization strategies are provided to maximize the power output.

2. Grating Structure with Equal-length Plates

2.1 Influence of electrode structure

The grating structure with two equal-length plates is first considered. In a grating TENG, the patterning of the triboelectric layer is essential in order to enable multiple charge separation cycles. On the other hand, patterning is not necessary for the attached electrodes. As shown in Fig. 1a, there are two choices available: a continuous plate electrode and a grating electrode, in which the electrodes are fabricated with the same grating as the dielectric layer. In this case, the electrical connection is realized through external circuits or electrode bars. These two electrode configurations will lead to different output performance.

To compare the output characteristics of the two grating structures with different electrode configurations, their finite element method (FEM) models were built and calculated using COMSOL. Since the width of grating TENGs is usually much larger than their thickness, 2D models were utilized to simplify the calculation. Two grating dielectrics with 50% duty cycle are placed as tribo-pairs (a pair of materials which will undergo contact electrification). Their half pitch is defined as l and the number of grating units in the top plate is defined as n. The total length of the top plate is L, such that $L = 2nl$. As an example, the case with two grating units (n = 2) was studied to illustrate the difference. (Detailed calculation parameters are listed in Table I.) Due to contact electrification, different signs of static charges (called tribo-charges) are distributed at the lower surface of Dielectric 1 and the upper surface of Dielectric 2. We assume that the tribo-charges are uniformly distributed on these surfaces with

a density of σ, which is our only assumption in our model. To verify this assumption, an experiment was conducted for the two units grating TENG with grating electrodes under constant velocity motion, which reaches very good agreement with theoretical anticipations, as shown in Fig. 2. (Detailed experimental design parameters and corresponding theoretical calculation is shown provided in ESI, Section 1). In order to simulate the relative-sliding motion in operation, the bottom dielectric is fixed and the top dielectric slides in the lateral direction, with the lateral displacement defined as x.

TABLE I

Parameters utilized in FEM calculations for comparing grating and plate electrodes

Structure Component	Parameter Utilized
Dielectric 1	$\varepsilon_{r1} = 4$, $d_1 = 220$ μm
Dielectric 2	$\varepsilon_{r2} = 2$, $d_2 = 220$ μm
Width of Dielectrics w	0.1 m
Total Length of the top plate L	0.16 m
Tribo-charge surface density σ	7 μCm^{-2}
Velocity v	1 ms^{-1}

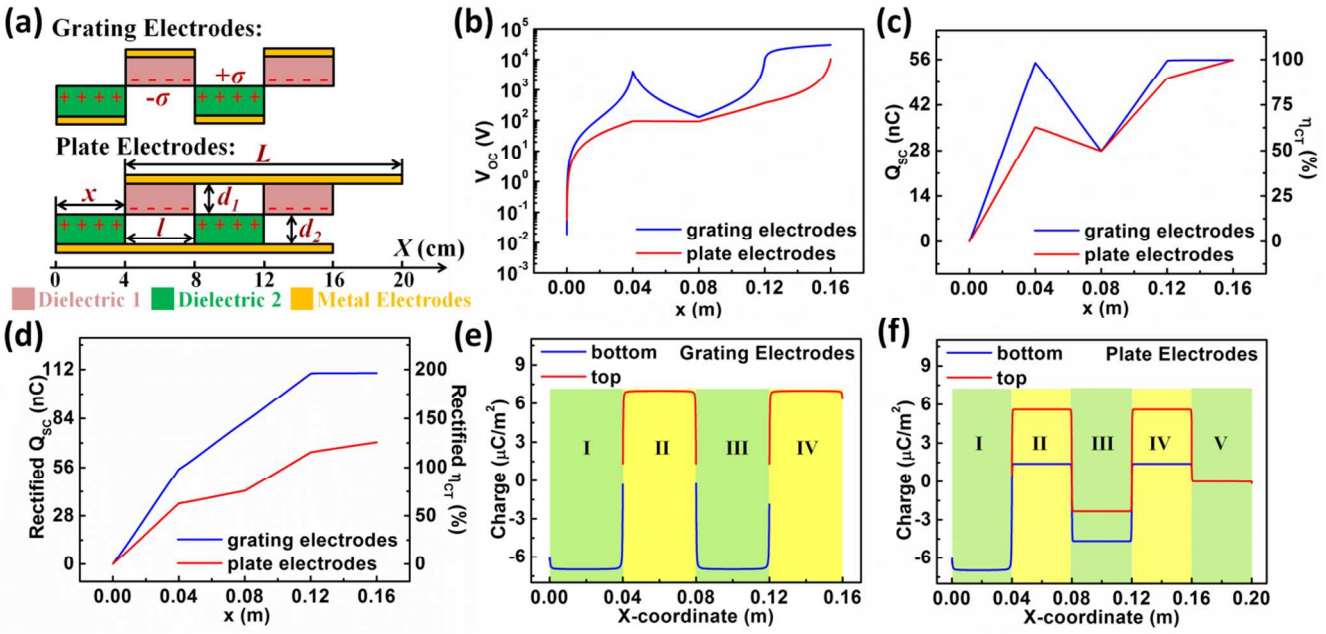

Fig. 1 Analysis and optimization of the electrode structure. (a) Structure of the FEM model for grating TENGs with grating electrodes and plate electrodes. (b-d) Calculated (b) open circuit voltage, (c) transferred charges at short circuit condition, and (d) rectified transferred charges at short circuit condition for grating TENGs with both grating electrodes and plate electrodes. (e-f) charge distribution at the metal electrodes for (e) grating electrodes and (f) plate electrodes at the case $x = l$.

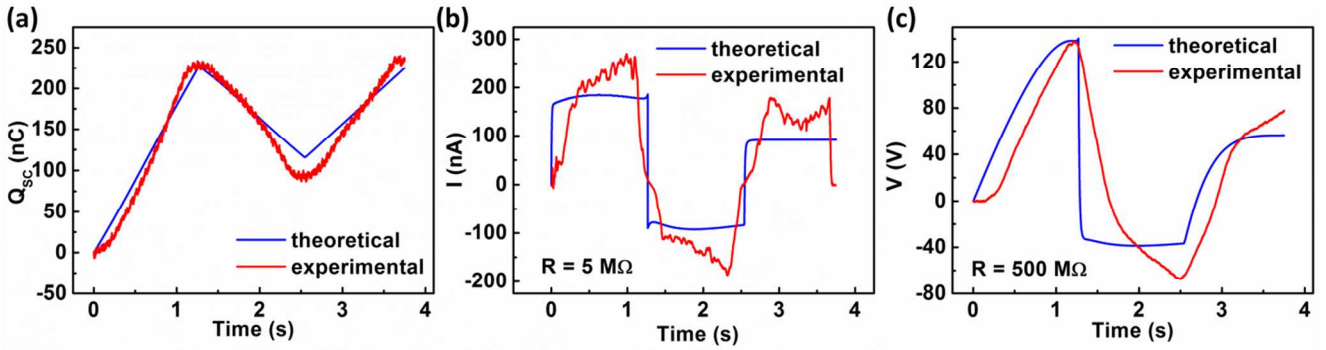

Fig. 2 Theoretical calculation results of real-time output of the grating TENG ($n = 2$, grating electrode structures) under constant velocity motion and comparison with the corresponding experimental results. (a) Comparisons of short circuit transferred charge from theoretical calculation and experiments. (b) Comparisons of current profiles from theoretical calculation and experiments at load resistance of 5 MΩ. (c) Comparisons of voltage profiles from theoretical calculation and experiments at load resistance of 500 MΩ.

The following FEM boundary conditions are applied to perform the calculation. The metal plates in each electrode group are assigned with the same electrical potential to reflect the external connection. The total charges in the top electrode is $Q+Q_0$ and those in the bottom electrode is $-Q-Q_0$, in which Q_0 (a constant) is the equilibrium charge level when the two plates fully overlap

with each other and Q is number of charges transferred during a certain displacement x. First, Q_0 is calculated from the number of charges transferred at $x = 0$ under short-circuit (SC) conditions. Then the open-circuit (OC) voltage (V_{OC}, defined as voltage under open circuit conditions when $Q = 0$) for different values of x is calculated by assigning the total charges on the electrodes to Q_0, where $Q = 0$. To calculate the SC transferred charges (Q_{SC}), the total charges transferred under SC ($Q_{net\text{-}SC}$) for different values of x are calculated. Then Q_{SC} is obtained by finding the difference between $Q_{net\text{-}SC}$ and Q_0. With these values of V_{OC} and Q_{SC} for different values of x, V_{OC} and Q_{SC} curves for the whole region are obtained through continuous fraction interpolation method.[16]

The profiles of V_{OC} and Q_{SC} generated by these two TENGs with different electrode structures are completely different, as shown in Fig. 1b-d. V_{OC}, Q_{SC}, and the charge transfer efficiency η_{CT} (defined as the ratio of Q_{SC} and the total amount of tribo-charges Q_{tribo}) of both structures show an oscillating trend, but those of the plate electrodes are always smaller than those of the grating electrodes. If the AC output is rectified to DC signal for storage, the TENG with grating electrodes would contribute a higher amount of accumulated charge. $\eta_{CT\text{-}rectified}$ after a full displacement cycle from the grating electrode structure can reach 200% while that from the plate electrode only reaches 126%. It should be noted that the reason that $\eta_{CT\text{-}rectified}$ is larger than 100% for both structures comes from the multiple cycles of charge separation, which is the key advantage of the grating structure. As for the open circuit voltage, V_{OC} after a full displacement cycle from the grating electrode can reach around 31 kV while that from the plate electrode only reaches around 10 kV. This set of comparisons clearly shows that the grating electrode is more effective in electricity generation than the plate electrode.

This difference in output characteristics results from the difference in charge distribution at the metal electrodes in these two electrode structures, as shown in Fig. 1e and f for the example case of $x = l$ under SC conditions. Q_{sc} equals half of the difference between the total amount of charge on top electrodes and on the bottom electrodes, which can be regarded as the sum of the contributions in all sub-regions (as marked in Fig. 1e and f). As an example, we can analyse the charge distribution in Region II and its contribution to Q_{sc} to elucidate the difference between these two electrode structures.

For the grating electrode, only the top electrode exists in this region. Therefore, the induced charge density on the top electrode is σ and its contribution to Q_{sc} is $\sigma wl/2$. For the plate electrode, both the top and bottom electrode exist in this region. A charge density of σ_T will be induced on the top electrode, and σ_B on the bottom. Thus its contribution to Q_{sc} is $(\sigma_T-\sigma_B)wl/2$. Since the electric field inside the metal electrodes is 0, the following relationship exists:

$$\sigma_T + \sigma_B = \sigma \quad (1)$$

In addition, because the voltage between the top and bottom electrodes is 0 under SC conditions, we will have:

$$\frac{\sigma_T}{\varepsilon_0}\frac{d_1}{\varepsilon_{r1}} = \frac{\sigma_B}{\varepsilon_0}d_2 \quad (2)$$

This equation indicates that σ_T and σ_B will have the same sign. From Equation 1, $(\sigma_T-\sigma_B)$ will be obviously smaller than σ. Thus, the contribution of the plate electrode in region II to Q_{sc} is smaller than that of the grating electrode structure. Likewise, in regions III and IV, their contribution to Q_{sc} of the plate electrode is also smaller than that of the grating electrode. As a result, the total Q_{SC} generated by the plate electrode will be smaller. Actually, for any arbitrary value of x, an approximate analytical solution for Q_{SC} of both electrode conditions can be derived, which is given in Table II and consistent with the results shown in Fig. 1c and d. (See ESI, Section 2 for a detailed derivation) From a more intuitive sense, this difference of charge distribution can also be explained from the different capacitance trend of the two structures. The capacitance for the grating electrode structure has an oscillating trend when x increases while the capacitance for the plate electrode monotonically decreases with the increase of x, as shown in Fig. S3. Therefore, through comparison of plate and grating electrode structures, it can be concluded that grating electrode structure is favourable for high output power. Thus, in the following discussion, we will mainly focus on TENGs with grating electrodes.

2.2 Output Characteristics

In order to fully understand the electricity generation process of a grating-TENG, the output characteristics should be systematically investigated. First, their V-Q-x relationship[17] needs to be derived. For all TENGs, the V-Q-x relationship is typically: [17]

$$V = -\frac{1}{C}\times Q + V_{OC} \quad (3)$$

where C is the capacitance between the two groups of electrodes and V_{OC} is the open circuit voltage when $Q = 0$. To obtain the semi-analytical V-Q-x relationship, interpolation of FEM calculation results was performed. Firstly, the voltage (V) at different values of Q and x was calculated. From the linear V-Q relationship at any given x, C and V_{OC} for any given x could be extracted. After that, a second-time interpolation utilizing a continuous fraction method was carried out to generate the interpolation function for the whole x region. In this grating structure, since the boundary condition of the FEM calculation changes in each cycle, the second-time interpolation needs to be conducted individually for each sub-region. The exact calculated results of the V-Q-x relationship are shown in ESI, Section 3.

The load characteristics can be calculated by combining the semi-analytical V-Q-x relationship and Ohm's law through the following equation:

$$R\frac{dQ}{dt} = V = -\frac{1}{C}\times Q + V_{OC} \quad (4)$$

This equation can be solved after specifying the motion process (defined as the specified $x(t)$ profile) and the boundary condition. The motion process will have no influence on V_{OC} and Q_{SC}, but will have an impact on time-related parameters (such as I_{SC}). As an example, the top electrode is assumed to move at a constant velocity (v), which can be shown as:

$$x = vt \quad \left(t < \frac{x_{max}}{v}\right) \quad (5a)$$

$$x = x_{max} \quad \left(t \geq \frac{x_{max}}{v}\right) \quad (5b)$$

TABLE II
Q_{SC} of grating and plate electrode structure under ideal conditions

	Grating Electrodes	Plate Electrodes
Step 1 ($0 \le x \le l$)	$2\sigma wx$	$\sigma wx\left(\frac{2d_2}{\frac{d_1}{\varepsilon_{r1}}+d_2}-\frac{\frac{d_2}{\varepsilon_{r2}}}{d_1+\frac{d_2}{\varepsilon_{r2}}}\right)$
Step 2 ($l \le x \le 2l$)	$\sigma w(3l-x)$	$\sigma w\left[x-l+(2l-x)\left(\frac{2d_2}{\frac{d_1}{\varepsilon_{r1}}+d_2}-\frac{\frac{d_2}{\varepsilon_{r2}}}{d_1+\frac{d_2}{\varepsilon_{r2}}}\right)\right]$
Step 3 ($2l \le x \le 3l$)	$\sigma w(x-l)$	$\sigma w\left[l+(x-2l)\frac{d_2}{\frac{d_1}{\varepsilon_{r1}}+d_2}\right]$
Step 4 ($3l \le x \le 4l$)	$2\sigma wl$	$\sigma w\left[2l+(x-4l)\frac{\frac{d_1}{\varepsilon_{r1}}}{\frac{d_1}{\varepsilon_{r1}}+d_2}\right]$

To specify the boundary condition of Q ($t = 0$) for Equation 4, we can take a general case that the device has stopped at the equilibrium position ($x = 0$) for a long time and electrostatic equilibrium has been reached before the motion process, so that Q ($t = 0$) is 0.

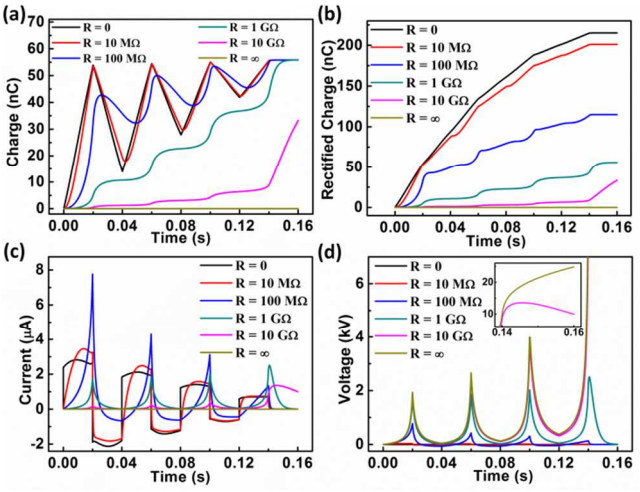

Fig. 3 Output characteristics of the equal-length grating TENG. (a-b) (a) Charge-time and (b) rectified charge-time relationship at different load resistances. (c) Current-time relationship at different load resistances. (d) Voltage-time relationship at different load resistances. The inset is the enlarged profile of the voltage at large resistances.

Using the calculation flow presented above, the load characteristics of an equal-length grating TENG with 4 units were calculated and plotted in Fig. 3. When R starts to increase from 0 (0 to about 10MΩ), the current and charge profiles stay close to those of the SC condition. As shown in Fig. 3a and b, in the low resistance region, charges transfer between the two electrodes in an oscillating manner, resulting in AC signals for both current and voltage. This oscillating charge transfer characteristics can lead to a much higher level of charge accumulation after rectification, which is usually n times the un-rectified charges, as shown in Fig. 3b. When R continues to increase (more than 10MΩ), the limitation of the resistor becomes more and more significant, so that the rectified charge curve shifts downward from the SC condition. The charge transfer characteristics gradually become monotonic and the current and voltage start to become DC in nature. As an interesting phenomenon, the maximum current will shoot high when R first increases. This is mainly because at this region, the increase of R will weaken the screening effect of the already transferred charges, which will possibly elevate the instantaneous driving force for the current from the unscreened potential difference.[18] As R approaches infinity, almost no electrons can transfer between the electrodes. Then, the current stays close to 0 and the voltage approaches the profile of V_{OC}.

2.3 Influence of number of grating units (n)

From the above study of the output characteristics, it can be observed that the number of grating units (n) has a direct impact on the total output characteristics. When n starts to increase from 1, the approximate ideal charge distribution is still satisfied because l is still much larger than the thickness of dielectrics. However, when n is increased to fairly large values and l is comparable with d_1 or d_2, the non-ideal edge effect is significant and cannot be neglected any longer. [17]

The influence of n in relatively small regions which satisfies the ideal conditions is first discussed. In this case, from the derivation in ESI Section 2 for the grating electrode structure, the instantaneous Q_{SC} and the short circuit current (I_{SC}) have the following relationships with n:

$$Q_{SC}=\frac{\sigma wL}{2}\left[\frac{k}{n}+\frac{2(n-k)}{L}(x-2kl)\right], 2kl \le x \le (2k+1)l \quad (k \in N) \quad (6a)$$

$$Q_{SC}=\frac{\sigma wL}{2}\left[1-\frac{2(n-k-1)}{L}(x-2kl-l)\right], (2k+1)l \le x \le (2k+2)l \ (k \in N) \quad (6b)$$

$$I_{SC}=\frac{\mathrm{d}Q_{SC}}{\mathrm{d}x}\frac{\mathrm{d}x}{\mathrm{d}t}=\sigma w(n-k)\frac{\mathrm{d}x}{\mathrm{d}t}, 2kl \le x \le (2k+1)l \quad (k \in N) \quad (7a)$$

$$I_{SC}=\frac{\mathrm{d}Q_{SC}}{\mathrm{d}x}\frac{\mathrm{d}x}{\mathrm{d}t}=-\sigma w(n-k-1)\frac{\mathrm{d}x}{\mathrm{d}t}, (2k+1)l \le x \le (2k+2)l \quad (k \in N) \quad (7b)$$

Therefore, the following equations give the accumulated charges ($Q_{SC\text{-}rectified}$) and charge transfer efficiency ($\eta_{CT\text{-}rectified}$) after rectification under SC conditions when a full displacement is finished:

$$Q_{SC,rectified}(x=L)=\frac{\sigma wL}{2}n \quad (8)$$

$$\eta_{CT,rectified}=\frac{Q_{SC,rectified}(x=L)}{Q_{tribo-total}}=n \quad (9)$$

From the above derivation, the peak value of I_{SC} and $Q_{SC\text{-}rectified}$ in the grating structure can be enhanced by n times through the subdivision process under ideal conditions, which is the most significant advantage of fabricating finer pitch structures.

To verify these results, a numerical calculation for a grating TENG under ideal conditions (L/d = 727.3, detailed calculation parameters are the same as shown in Table I) is performed and the results are shown in Fig. 4a-d. The numerically calculated results are consistent with the theoretical analysis above. When n increases, the number of charge transfers increases as a response, which significantly elevates the amount of accumulated charges after rectification. In addition, the slope of $Q_{SC} - t$ curve also

increases with n, leading to an enhancement of I_{SC}, as shown in Fig. 4b. But as for voltage, since finer pitch results in a significant increase in capacitance when the top dielectrics and bottom dielectrics are fully separated, the peak value of V_{OC} at larger n significantly drops while the peak value of Q_{SC} remains almost the same, which is determined by the following equation: [17, 19]

$$V_{OC} = \frac{Q_{SC}}{C} \qquad (10)$$

Such a change in V_{OC} is shown in Fig. 4c. However, the total energy generated is more complicated, as it is determined by both the current and the voltage. Fig. 4d shows the energy generated by 3 TENG structures with different n in one full back-and-forth cycle under different load resistances (detailed information about the calculation for energy is shown in ESI, Section 4). The following conclusions can be reached by comparing the curves shown in Fig. 4d. First, a finer pitch can generate more energy in the low resistance range, where the energy is mainly dominated by I_{SC}. However, a wider pitch can generate more energy in the high resistance range, where the generated energy is mainly determined by V_{OC}. The optimum resistance (the resistance at which the total energy is maximized) decreases with n, due to the higher I_{SC} and lower V_{OC}. [18] Considering the peak value of the harvested energy (in Fig. 4d), a finer pitch doesn't significantly improve the output, as V_{OC} decreases more significantly than I_{SC} increases for the equal-length grating TENGs.

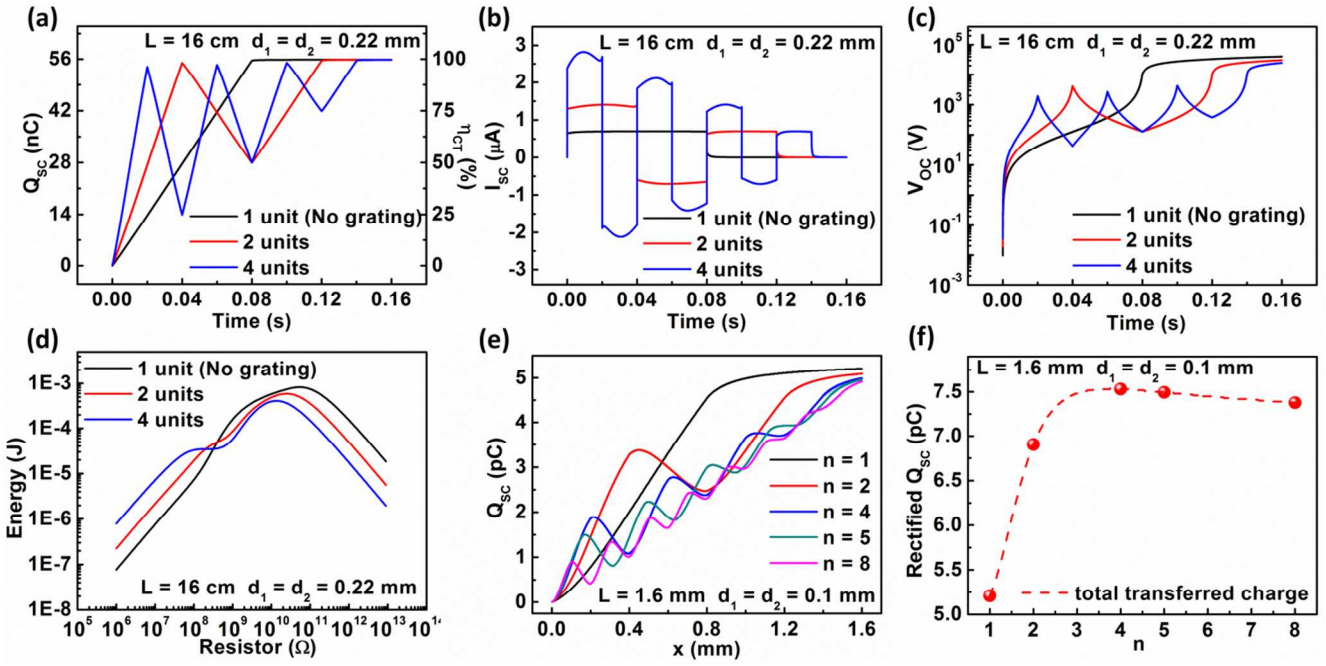

Fig. 4 Influence of number of pitches (n) on the output performance of equal-length grating TENGs. (a-d) Influence of n under ideal condition. (a) The relationship between transferred charges at short circuit and time at different n. (b) The relationship between current at short circuit and time at different n. (c) The relationship between open circuit voltage and time at different n. (d) The relationship between generated energy and load resistance at different n. (e-f) Influence of n when edge effect dominates the output characteristics. (e) Short circuit transferred charges profile with moving distance at different n. (f) Total short circuit transferred charges relationship with n.

When n continues to increase to very large values, the aspect ratio of each unit will be further lowered and the non-ideal edge effect cannot be neglected. To study the influence of this non-ideal effect, a numerical calculation for grating TENGs with a small L/d ratio of 16 was conducted, as shown in Fig. 4e and f. (Detailed calculation parameters are shown in Table III.) At this aspect ratio, although the times of charge transfer increases with increasing values of n, the peak value of Q_{SC} in each period is far smaller than that of Q_{tribo}. Especially when n is larger than 5, the transfer of charges is unidirectional after the first few cycles, so $Q_{SC\text{-}rectified}$ doesn't have a multiplication effect in these cycles. As a result, $Q_{SC\text{-}rectified}$ starts to drop with an increasing value of n. Because of the reverse influence of n in the two different regions, there is an optimum value of n that yields the maximum $Q_{SC\text{-}rectified}$. As shown in Fig. 4f, for a total geometric aspect ratio, the optimum value of n is about 4, in which the geometric aspect ratio of each unit is 2. This calculation shows that it is critically important to have this optimum value of n to generate the optimum charge when this kind of TENG is being used to charge a battery or capacitor.

TABLE III
PARAMETERS UTILIZED IN THE FEM CALCULATION FOR ILLUSTRATING NON-IDEAL EFFECT FOR THE EQUAL-LENGTH GRATING TENGS.

Structure Component	Parameter Utilized
Dielectric 1	$\varepsilon_{r1} = 4$, $d_1 = 100$ μm
Dielectric 2	$\varepsilon_{r2} = 2$, $d_2 = 100$ μm
Width of Dielectrics w	1 mm
Total Length of the top plate L	1.6 mm
Tribo-charge surface density σ	7 μCm^{-2}
Velocity v	1 ms^{-1}

3. Grating TENGs with unequal-length plates

In the above section, we mainly discussed the design of grating TENGs with two plates of equal length. In such a structure, the top units will gradually slide out from the bottom grating due to lateral displacement. This feature is favourable for a high open-circuit voltage (because of the small side capacitance), but results in non-periodic signals. To avoid this situation, the length of the bottom plate that is stationary during operation can be increased to fully cover the sliding region of the top plate, which forms another structure of grating TENGs with plates of unequal length. As a typical example, the length of the bottom part is set to $2L$, which is twice the length of top part. Thus, the sliding displacement is maintained as L. In this structure, because of the charge conservation in contact electrification, the tribo-charge density of Dielectric 1 (-2σ) is twice as high as that of Dielectric 2 (σ). Because Dielectric 1 is always sliding within the range of Dielectric 2, Q_{SC}, V_{OC} and C will be periodic. In addition, the Q_{SC}, V_{OC} and C curves all have mirror symmetry in each single period, which can be mathematically shown by the following set of equations.

$$V_{OC}(x+2kl) = V_{OC}(x) \quad (11a)$$

$$V_{OC}(2kl-x) = V_{OC}(x) \quad (11b)$$

$$C(x+2kl) = C(x) \quad (11c)$$

$$C(2kl-x) = C(x) \quad (11d)$$

$$Q_{SC}(x+2kl) = Q_{SC}(x) \quad (11e)$$

$$Q_{SC}(2kl-x) = Q_{SC}(x) \quad (11f)$$

Because of the periodicity and mirror symmetry, we only need to simulate the TENG for its first half period. As for the electrode structure, the grating electrode still provides a better performance than the plate electrode in this case, which can be obtained from a similar discussion and derivation as above. Therefore, in the following discussion, we mainly focus on the unequal-length grating TENGs with the grating electrode.

3.1 Influence of dielectric thickness

Unlike equal-length grating TENGs, the choice of dielectric thickness can significantly influence Q_{SC}. Under ideal conditions (l/d is sufficiently large), Q_{SC} and η_{CT} of this grating TENG can be given by:

$$Q_{SC} = \left(2 - \frac{1}{1+\frac{d_1\varepsilon_{r2}}{d_2\varepsilon_{r1}}}\right) n\sigma w(x-2kl),$$

$$2kl \le x \le (2k+1)l \quad (k \in N) \quad (12a)$$

$$Q_{SC} = \left(2 - \frac{1}{1+\frac{d_1\varepsilon_{r2}}{d_2\varepsilon_{r1}}}\right) n\sigma w(2kl+2l-x),$$

$$(2k+1)l \le x \le (2k+2)l \quad (k \in N) \quad (12b)$$

$$\eta_{CT} = \left(1 - \frac{1}{2}\frac{1}{1+\frac{d_1\varepsilon_{r2}}{d_2\varepsilon_{r1}}}\right)\frac{x-2kl}{l},$$

$$2kl \le x \le (2k+1)l \quad (k \in N) \quad (13a)$$

$$\eta_{CT} = \left(1 - \frac{1}{2}\frac{1}{1+\frac{d_1\varepsilon_{r2}}{d_2\varepsilon_{r1}}}\right)\frac{2kl+2l-x}{l},$$

$$(2k+1)l \le x \le (2k+2)l \quad (k \in N) \quad (13b)$$

where n is defined as the number of units in top dielectrics and detailed derivation is shown in ESI, Section 5. From the above equations, it is observed that Q_{SC} and η_{CT} decrease dramatically if the ratio of d_2/d_1 increases, which is because of the non-zero value of Q_0 from the not totally overlapped surface when $x = 0$. To minimize this effect, as shown in Equation 12, the ratio d_2/d_1 needs to be reduced. An effective design is to eliminate the dielectric layer on the bottom plate and use a conductive material as both electrode and tribo-layer, in which d_2 can be regarded as 0. In order to validate this, the performance of this conductor-to-dielectric structure ($d_2 = 0$) where $n = 4$ is compared with the dielectric-to-dielectric TENG structure ($d_2 = d_1$) as shown in Fig. 5b-c. The detailed parameters for this calculation are listed in Table IV. The peak values of Q_{SC}, η_{CT} and V_{OC} from the conductor-to-dielectric TENG are all higher than the dielectric-to-dielectric TENG. Thus, the conductor-to-dielectric design is favourable for efficient charge transfer, from the point of view of device structure. Therefore, we will mainly focus on this design in the following discussion.

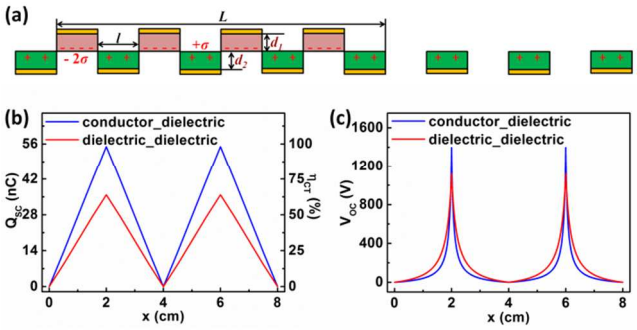

Fig.5 Influence of the dielectric thickness on the performance of the unequal-length grating TENGs. (a) FEM model for unequal-length grating TENGs. (b-c) Comparison of conductor-to-dielectric and dielectric-to-dielectric unequal-length grating TENGs on (b) short circuit transferred charges and (c) open circuit voltage.

TABLE IV
PARAMETERS FOR FEM CALCULATION FOR UNEQUAL-LENGTH GRATING TENGS

Structure Component	Dielectric-to-dielectric unequal-length grating TENGs	Conductor-to-dielectric unequal-length grating TENGs
Dielectric 1 Dielectric 2	$\varepsilon_{r1}=4$, $d_1=220$ μm $\varepsilon_{r2}=2$, $d_2=220$ μm	$\varepsilon_{r1}=4$, $d_1=220$ μm *Metal*, $d_2=0$ μm
Width of Dielectrics w	0.1 m	0.1 m
Total Length of the top plate L	0.16 m	0.16 m
Tribo-charge surface density at the bottom dielectric surface σ	3.5 μCm^{-2}	3.5 μCm^{-2}
Velocity v	1 ms^{-1}	1 ms^{-1}

3.2 Output Characteristics

Besides its basic characteristics, the load performance of the unequal-length grating TENG was studied as well. First, we need to specify the motion process and the boundary condition. We still choose the simplest case—movement at a constant velocity. However, due to the intrinsic periodicity, output from any initial boundary condition will gradually converge to a periodic output wave after the first few periods, which is the steady-state (Fig. S7 and ESI, Section 6). The convergence time increases when the load resistance increases, but as long as the load resistance is not too large, convergence is achieved in less than 10 periods. The periodic boundary conditions are shown as:

$$Q(t=0) = Q\left(t = \frac{2l}{v}\right) \qquad (14)$$

At a constant velocity, this boundary condition can also be given by:

$$\begin{aligned} &Q(t=0) \\ &= \frac{\exp\left(-\frac{2}{Rv}\int_0^l \frac{1}{C(x)}dx\right)}{1-\exp\left(-\frac{2}{Rv}\int_0^l \frac{1}{C(x)}dx\right)} \frac{1}{Rv}\int_0^l V_{OC}(x)\exp\left(\frac{1}{Rv}\int_0^x \frac{1}{C(z)}dz\right)dx \\ &+ \frac{1}{1-\exp\left(-\frac{2}{Rv}\int_0^l \frac{1}{C(x)}dx\right)} \\ &* \frac{1}{Rv}\int_0^l V_{OC}(x)\exp\left(-\frac{1}{Rv}\int_0^x \frac{1}{C(z)}dz\right)dx \end{aligned} \qquad (15)$$

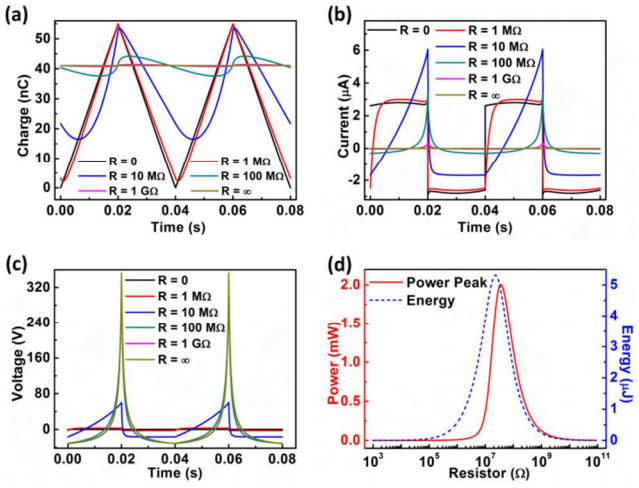

Fig.6 Output characteristics of the unequal-length grating TENGs under periodic boundary condition. (a) Transferred charge-time relationship at different load resistances. (b) Current-time relationship at different load resistances. (c) Voltage-time relationship at different load resistances. (d) Extracted maximum power and total energy relationship with load resistance in one period.

For a more detailed derivation see ESI, Section 6. With the above periodic boundary conditions, numerical calculations of the load performance can be easily performed. Fig. 6 shows the results from an unequal-length grating TENG for n = 4. The output at any resistance load is in the shape of periodic waves. Besides, the current and voltage are both AC signals and the integration of the current and voltage in the entire period is 0. When R is small, due to the low resistance of charge transport, the output is quite similar to that of the short circuit condition. The charge transfer curve is almost linear in each half period and the current curve is close to a square wave. When R increases, the limitation to the charge transport becomes more and more significant, leading to a smaller oscillation magnitude of the charge transfer curve. As R continues to increase, the charge transfer curve approaches a constant value and the current approaches 0. At the same time, the voltage curves converge to the curve with the same shape as V_{OC}, as shown in Fig. 6c. It should be noted that this voltage curve at infinitely-large resistance is not the same as V_{OC}. V_{OC} is calculated through the boundary condition of $Q(t=0) = 0$, but this curve in Fig. 6c is obtained utilizing the periodic boundary condition in which $Q(t=0)$ is given by Equation 15. Therefore, the V_{OC} curve is always positive, but this curve with periodic boundary condition gives an AC signal. From the above analysis, this kind of grating TENG also shows the three-working-region behaviour. In the middle range of R, the peak transit power is reached and the maximum energy from a single cycle can be reached as well, with the two corresponding optimum resistances approaching one another.

3.3 Influence of number of grating units (n)

With the above basic understanding of the output characteristics of the unequal-length grating TENG, we can discuss the influence of the most important design parameter: the number of grating units. The output performance of a TENG with different n is calculated and plotted in Fig. 7. When n increases in the small region, since the aspect ratio of each grating unit (l/d_1) is still large enough, the transferred charge amount in one half-cycle stays almost the same as Q_{tribo}. Therefore, since the total accumulated charges ($Q_{SC,rectified}(x = L)$) equals to $2n$ times the amount of transferred charge in one half-cycle, the total accumulated charges and average current magnitude increase quasi-linearly with n in its small value region, as shown in Fig. 7b. However, when n continues to increase, the non-ideal edge effect becomes much more significant due to the decrease in the aspect ratio in each unit, resulting in a decreased number of transferred charges in each half-cycle. Although the number of charge transfer cycles still increases, the elevation slope of the total accumulated charges decreases dramatically. When n is sufficiently large, the slope of the total accumulated charges is close to 0 and the average current no longer increases. Additionally, finer pitches also contribute to a significant increase in the side capacitance between the top and bottom electrode. Therefore, in Equation 10, V_{OC} will significantly drop with increased n, as shown in Fig. 7d. Unlike the case in equal-length grating TENG, the V_{OC} and Q_{SC} curves in each half-cycle are always monotonic, even when n is sufficiently large. The peak value of the V_{OC} and Q_{SC} curves are always in the middle position of each period. With these characteristics, unequal-length grating TENGs can have applications as a self-powered sensor for actively measuring displacement and velocity with high accuracy and resolution. [20]

With the above basic output characteristics, the load performance of these TENGs was numerically calculated, from which the total harvested energy was plotted corresponding to different load resistances, as shown in Fig. 7e and f. Since finer pitches yield a

larger I_{SC} but a smaller V_{OC}, the optimum resistance shifts significantly to lower values. [18] In addition, unlike the equal-length grating TENGs, an optimum value of n exists (about 108 through interpolation) for the unequal-length grating TENGs, which yields the maximum total harvested energy. With this optimum n, the aspect ratio is 3.37 for each grating unit. This optimum n originates from the complicated behaviour of V_{OC} and I_{SC}. When n first increases, the average value of I_{SC} increases more significantly than V_{OC} decreases, so the harvested energy will increase. However, when n continues to increase, the growth rate of I_{SC} decreases dramatically because of the non-ideal edge effect. Therefore, the total harvested energy starts to decrease when the decreasing V_{OC} becomes the dominant factor.

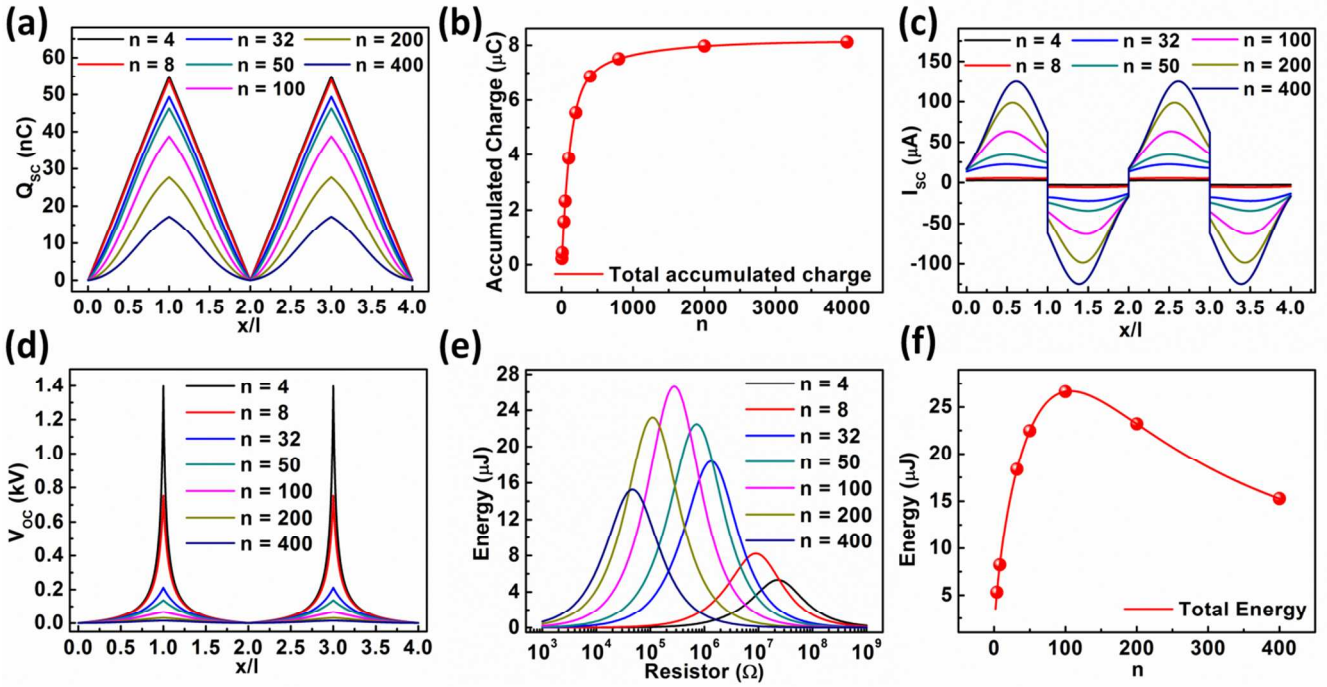

Fig.7 Influence of the number of pitches (n) on the output performance of unequal-length grating TENGs. (a) Short circuit transferred charges curves of grating TENGs with different n. (b) Extracted total short circuit transferred charges when a full separation is reached ($x = L$). (c) Short circuit current profiles of grating TENGs with different n. (d) Open circuit voltage profiles of grating TENGs with different n. (e) Total generated energy profiles when a full separation is reached ($x = L$) under different load resistance and different n condition. (f) Influence of n on the total generated energy when a full separation is reached ($x = L$).

This critical aspect ratio for the individual dielectric unit that yields the largest total energy mainly depends on the motion process and the relative dielectric constant of Dielectric 1. We can take the unequal-length grating TENG at constant velocity as an example. In this condition, this critical aspect ratio is only dependent on the relative dielectric constant of Dielectric 1 (independent on d_1, L, and v). We first studied the influence of d_1. Consider two unequal-length grating TENGs (A and B) with different Dielectric 1 thicknesses of d_{1A} and d_{1B} ($d_{1A} = k^* d_{1B}$, k is defined as a scale factor), respectively. Their total length L, the aspect ratio of each grating unit, and the material of Dielectric 1 are all the same. Therefore, the following equations need to be satisfied.

$$n_B = kn_A, \quad (16) \qquad l_B = \frac{1}{k} l_A, \quad (17)$$

Because of the inherent periodicity of this structure, the electric field distribution in each grating unit is completely identical. Since the electric field distribution of one grating unit is mostly determined by its surrounding elements, increasing n while maintaining the same aspect ratio will not affect the electric field distribution. Moreover, with the same aspect ratio in each grating unit, the distribution of the electric field is scaled in space, without a change in electric field strength. Therefore, the capacitance in each grating unit remains the same while V_{OC} changes by a factor of k since the integration distance of the electric field is scaled by k. For an n unit system, the total capacitance (C) still needs to be multiplied by n. Thus, the V_{OC} and C of the two TENGs have the following relationships.

$$V_{OC,B}(x) = \frac{1}{k} V_{OC,A}(kx), \quad (0 \le x \le l_B) \quad (18);$$

$$C_B(x) = kC_A(kx), \quad (0 \le x \le l_B) \quad (19)$$

Therefore, their V-Q-x relationship can be expressed as:

$$V_A = -\frac{1}{C_A(x)} Q_A + V_{OC,A}(x) \qquad (20a)$$

$$V_B = -\frac{1}{C_B(x)} Q_B + V_{OC,B}(x) = -\frac{1}{kC_A(kx)} Q_B + \frac{1}{k} V_{OC,A}(kx)$$

(20b)

Now we consider one grating TENG A connected to a load resistance R_A and the other grating TENG B connected to a load resistance R_B with the condition that R_A is k^2 times as large as R_B. At this load condition, the differential equations for these two

grating TENGs can be given by:

$$R_A \frac{dQ_A}{dt} = -\frac{1}{C_A(vt)} Q_A + V_{OC,A}(vt) \quad (21a)$$

$$\frac{1}{k^2} R_A \frac{dQ_B}{dt} = -\frac{1}{kC_A(kvt)} Q_B + \frac{1}{k} V_{OC,A}(kvt) \quad (21b)$$

In addition, at this load condition, the periodic boundary condition for these two TENGs can be proven to be the same through Equation 15 (detailed proof shown in ESI, Section 7). Thus, the above differential equations can be analytically solved and their output characteristics have a scalar relationship as well, which can be elucidated by the following equations (detailed proof shown in ESI, Section 7).

$$Q_B(t) = Q_A(kt), \quad \left(0 \le t \le \frac{l_B}{v}\right) \quad (22)$$

$$I_B(t) = \frac{dQ_B}{dt} = kI_A(kt), \quad \left(0 \le t \le \frac{l_B}{v}\right) \quad (23)$$

$$V_B(t) = I_B(t)R_B = \frac{1}{k} V_A(kt), \quad \left(0 \le t \le \frac{l_B}{v}\right) \quad (24)$$

The relationship for the energy generated in the whole sliding process can be given by:

$$\begin{aligned} E_B &= 2n_B \int_0^{l_B/v} I_B(t)V_B(t)dt = 2kn_A \int_0^{l_A/(kv)} I_A(kt)V_A(kt)dt \\ &= 2n_A \int_0^{l_A/v} I_A(t)V_A(t)dt \\ &= E_A \end{aligned} \quad (25)$$

Therefore, the total energy harvested for grating TENG B at load resistance R_B is completely identical to that of grating TENG A at load resistance k^2R_B. Thus, the optimum resistance of grating TENG A is also k^2 times larger than that of grating TENG B. Moreover, when TENG A and TENG B are both at their optimum load, their maximum total harvested energy is the same. Since the maximum harvested energy from TENG A and TENG B is the same for any arbitrary aspect ratio, the optimum grating aspect ratio is independent of d_l in this motion process.

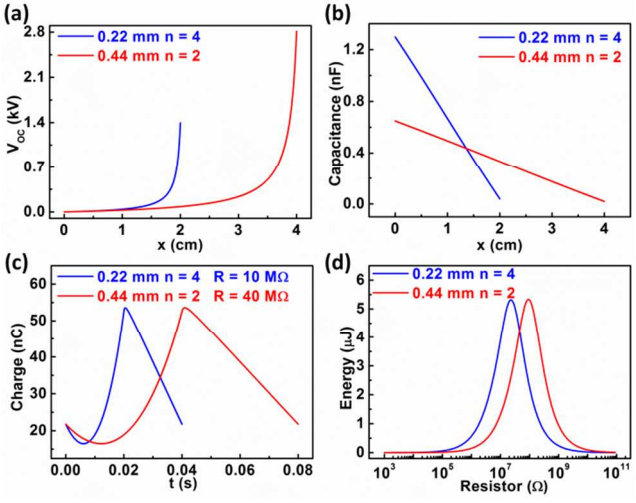

Fig.8 Comparison between unequal-length grating TENGs with d_l = 0.22 mm, n = 4 and d_l=0.44 mm, n = 2 (a) Open circuit voltage comparison. (b) Capacitance comparison. (c) Charge-time relationship comparison with appropriate load resistances. (d) Total generated energy comparison at different load resistances.

To verify the above theoretical prediction, the numerical calculation for k = 2 is performed. The detailed calculation parameters are the same as those listed in Table IV except as specified in Fig. 8. Maintaining the same aspect ratio, their V_{OC} and capacitance curves both have the same shape, which shows the same results as Equation 18 - 19. With the periodic boundary condition and load resistances satisfying the relationship of the scale factor (k^2), their charge transfer curves have the same profile. Their total energy curves have almost the same shape and peak value, with only a translation along the resistance axis. Thus, the numerical calculation results are completely consistent with our theoretical predictions, which elucidates that the optimum unit aspect ratio in each unit is independent on d_l at this condition. Similarly, the change of L and velocity v will not influence the optimum unit aspect ratio either (detailed proof shown in ESI, Section 8 and 9). Therefore, the optimum aspect ratio mainly depends on the relative dielectric constant of Dielectric 1 and the motion type.

4. Material selection and its relationship with structural design

Besides the structural optimization strategy we proposed above, another factor in improving TENG performance is to optimize the tribo-pair materials. The major effect of changing tribo-pair materials on the output performance is the change in tribo-charge density (σ). Additionally, different materials will lead to different relative dielectric constants as well, but this will have a negligible effect on the output performance.

First, different tribo-pair materials will result in different levels of tribo-charge density, which will strongly influence the output performance. Due to the superposition principle of electric potential, V_{OC} in Equation 3 is proportional to σ while the capacitance term (C) is independent on σ. Thus, the output parameters (including Q, V, and I) solved from Equation 4 are all directly proportional to σ. Therefore, σ will only affect the magnitude of the output parameters, but not their shape with respect to both time or load resistance. Therefore, all the structural parameters (including optimum resistance and optimum aspect ratio) have no dependence on σ. Thus, the structural design is completely decoupled from σ, which is the main parameter to target while selecting tribo-pair materials.

Besides, as shown in the above discussion of grating electrode TENGs, material selection will have an impact on the structural parameters by changing the effective dielectric thickness (defined as d_i/ε_{ri}). However, this effect is always trivial in tribo-pair material selection because of the following two reasons. First, the relative dielectric constant of the most commonly utilized tribo-pair materials does not vary too much (always in the range of 2-4), so compared to the influence of σ, changing these dielectric constants does not significantly affect the output performance. Second, as the effective dielectric thickness directly affects the structural parameters, the impact of changing the relative

dielectric constants can always be compensated by changing the dielectric thickness on the same scale. Thus, in practical TENG design, optimizing σ is always the only target of material selection, which is a fully decoupled process from structural optimization.

To choose materials that can provide a higher σ, we need to select one material which is tendency to lose electrons and the other one which is tendency to gain electrons. However, because the detailed mechanism of contact electrification is still under investigation, we can only rely on some empirical results, tabulated in the triboelectric series.[21] Tribo-pair materials are always selected from the two ends of the triboelectric series. Additionally, nanostructures on the surface of the tribo-pair materials have been experimentally proven to be an effective way to improve σ.[12]

5. Conclusions

In this paper, a theoretical study on grating triboelectric nanogenerators is performed, which outlines their design strategies. There are generally two different categories of grating TENGs with different output characteristics: grating TENGs with equal and unequal plate length. For each of these two categories, besides the study of the basic output profile, we performed an in-depth discussion on the influence of electrode structures, number of grating units, and thickness of the dielectric layers for the unequal plate structure. As for the electrode structure, grating electrodes always lead to a better performance than plate electrodes for both of these categories. As for the most important parameters of grating TENGs—the number of grating units, our theoretical calculation clearly indicates that increasing the number of grating units to get a finer pitch will generally improve the output performance. However, when the pitch is very fine, the edge effect begins to dominate, resulting in degradation of performance when the number of units continues to increase. Thus, there exists an optimum number of grating units, and an optimum unit aspect ratio that mainly depends on the materials dielectric constant and the motion type. These are important parameters to consider for future structural design. As for the dielectric thickness in the unequal length design, the thickness of the dielectric of the longer plate should be much smaller than that of the shorter plate. The theoretical work presented here is the first in-depth investigation of the working principle of the grating TENG. The discussion about the structural design and optimization can serve as a guideline for rational design to maximize electrical output.

Acknowledgements

Research was supported by U.S. Department of Energy, Office of Basic Energy Sciences under Award DEFG02-07ER46394, NSF, MURI, and the "thousands talents" program for pioneer researcher and his innovation team, China. The authors also thank Yannan Xie for his technical assistance.

Notes and references

[a] *School of Material Science and Engineering, Georgia Institute of Technology, Atlanta, Georgia 30332-0245, United States, Email: zlwang@gatech.edu*

[b] *Beijing Institute of Nanoenergy and Nanosystems, Chinese Academy of Sciences, Beijing, China*

† Electronic Supplementary Information (ESI) available. See DOI: 10.1039/b000000x/

‡ S. Niu, S. Wang, and Y. Liu contributed equally to this work

1. S. P. Beeby, R. N. Torah, M. J. Tudor, P. Glynne-Jones, T. O'Donnell, C. R. Saha and S. Roy, *J. Micromech. Microeng.*, 2007, **17**, 1257-1265.
2. C. R. Saha, T. O'Donnell, N. Wang and R. McCloskey, *Sen. Actua. A*, 2008, **147**, 248-253.
3. Y. Suzuki, *IEEJ T. Electr. Electr.*, 2011, **6**, 101-111.
4. O. D. Jefimenko and D. K. Walker, *IEEE T. Ind. Appl.*, 1978, **14**, 537-540.
5. H. W. Lo and Y. C. Tai, *J. Micromech. Microeng.*, 2008, **18**.
6. A. Khaligh, P. Zeng and C. Zheng, *IEEE T. Ind. Electron.*, 2010, **57**, 850-860.
7. L. S. McCarty and G. M. Whitesides, *Angew. Chem. Int. Edit.*, 2008, **47**, 2188-2207.
8. R. G. Horn, D. T. Smith and A. Grabbe, *Nature*, 1993, **366**, 442-443.
9. R. G. Horn and D. T. Smith, *Science*, 1992, **256**, 362-364.
10. H. T. Baytekin, A. Z. Patashinski, M. Branicki, B. Baytekin, S. Soh and B. A. Grzybowski, *Science*, 2011, **333**, 308-312.
11. F. R. Fan, Z. Q. Tian and Z. L. Wang, *Nano Energy*, 2012, **1**, 328-334.
12. F. R. Fan, L. Lin, G. Zhu, W. Z. Wu, R. Zhang and Z. L. Wang, *Nano Lett.*, 2012, **12**, 3109-3114.
13. S. H. Wang, L. Lin, Y. N. Xie, Q. S. Jing, S. M. Niu and Z. L. Wang, *Nano Lett.*, 2013, **13**, 2226-2233.
14. G. Zhu, J. Chen, Y. Liu, P. Bai, Y. S. Zhou, Q. S. Jing, C. F. Pan and Z. L. Wang, *Nano Lett.*, 2013, **13**, 2282-2289.
15. L. Lin, S. H. Wang, Y. N. Xie, Q. S. Jing, S. M. Niu, Y. F. Hu and Z. L. Wang, *Nano Lett.*, 2013, **13**, 2916-2923.
16. J. Stoer and R. Bulirsch, *Introduction to numerical analysis*, Springer, New York, 2002.
17. S. M. Niu, Y. Liu, S. H. Wang, L. Lin, Y. S. Zhou, Y. F. Hu and Z. L. Wang, *Adv. Mater.*, 2013, **25**, 6184-6193.
18. S. M. Niu, S. H. Wang, L. Lin, Y. Liu, Y. S. Zhou, Y. F. Hu and Z. L. Wang, *Energ. Environ. Sci.*, 2013, **6**, 3576-3583.
19. S. M. Niu, Y. Liu, S. H. Wang, L. Lin, Y. S. Zhou, Y. F. Hu and Z. L. Wang, *Adv. Funct. Mater.*, DOI: 10.1002/adfm.201303799
20. Y. S. Zhou, G. Zhu, S. M. Niu, Y. Liu, P. Bai, Q. S. Jing and Z. L. Wang, *Adv. Mater.*, 2014, **26**, 1719-1724.
21. A. F. Diaz and R. M. Felix-Navarro, *J. Electrostat.*, 2004, **62**, 277-290.